

An analysis of the turbulence in the central region of M 42 through structure functions

G.A. Anorve-Zeferino,¹★

¹École Polytechnique, Route de Saclay, Palaiseau, 91128, France

Accepted XXX. Received YYY; in original form ZZZ

ABSTRACT

Here, we analyse the character of the turbulence of the Huygens Region in the Orion Nebula (M 42) using structure functions. We compute the second order structure function of a high resolution velocity map in H α obtained through the *MUSE* instrument. Ours is one of the few works that follows a mathematically sound methodology for calculating the second order structure function of astronomical velocity fields. Because of that our results will be useful for future comparisons with other studies of M 42 or other regions. We first analyse the Probability Distribution Function (PDF) and found it consistent with those resulting from numerical simulations of solenoidal turbulence. After a further analysis of the data, we found two possible separate motions or at least regimes in the region. This is confirmed later through the calculation of several filtered structure functions. We found that the turbulence in the Huygens Region is between the Kolmogorov regime ($S_2 \propto \delta r^{2/3}$) and the Burgers regime ($S_2 \propto \delta r$). We found that the turbulence in the region consists on two flow regimes that reproduce a generalised Larson’s Law, $S_2 \sim \delta r^{0.74-0.76}$.

Key words: (ISM:) H II regions – (ISM:) Herbig-Haro objects – hydrodynamics – ISM: general – ISM: kinematics and dynamics – turbulence

1 INTRODUCTION

The current standard view is that turbulence is ubiquitous in H II regions, molecular clouds and star forming regions in general; see [Klessen \(2001\)](#), [Glover et al. \(2010\)](#), [Tremblin et al. \(2012\)](#), [Mellema et al. \(2016\)](#) and references therein. The internal motions of the gas that comprise them are dominated by supersonic turbulence, the radiation field of young massive stars and also magnetic fields trapped within the ISM, see [Gritschneider et al. \(2009\)](#) and [Federrath & Klessen \(2012\)](#). Supersonic turbulence can be driven by powerful superwinds [[Anorve-Zeferino, Tenorio-Tagle & Silich \(2009\)](#) and [Anorve-Zeferino \(2016\)](#)], the feedback from UV radiation, magnetic pressure, magnetic rotational instability, galactic shear, SNe explosions, gravity/accretion, cloud-cloud collisions, spiral-arm compression and some others, all of which can generate turbulence which can provide important support against gravitational collapse in molecular clouds and H II regions and also control their star formation, see [Hartquist, Pittard & Falle \(2007\)](#) and [Federrath et al. \(2017\)](#).

Nevertheless, the velocity field of H II regions and molecular clouds can only be observed in projection since we only have line-of-sight information that can be synthesized

in position-position-velocity (PPV) cubes constructed after the detection and analysis of emission lines. Nevertheless, this provides the opportunity of knowing at least the line of sight motion inside these regions and try to extract information through diverse methods in order to unveil the physics behind it. One of such methods is the use of (transversal) S_p -structure functions to try to diagnose turbulence. In this Paper, we obtain the second order structure function of the Huygens Region in the Orion Nebula using the centroid velocities of its H α emission lines.

The p-th order transversal S_p -structure function is given by¹

$$S_p(\delta r) = \langle [u(\vec{\mathbf{r}} + \vec{\delta\mathbf{r}}) - u(\vec{\mathbf{r}})]^p \rangle, \quad (1)$$

where the braces $\langle \rangle$ indicate "average over the ensemble of realisations", u is the line-of-sight velocity and $\vec{\mathbf{r}}$ is the transversal radial vector. For the case of the PPV cubes here analysed, u corresponds to the expansion velocity derived from H α lines. For (quasi-)static fields, $\langle \rangle$ is a type of spatial averaging. At the time of calculating structure functions,

¹ see [Federrath, Klessen & Schmidt \(2009\)](#) and [Federrath et al. \(2010\)](#) for examples of longitudinal structure functions of density and velocity fields from numerical simulations of compressive and solenoidal turbulence

★ E-mail: Alex.Anorve@protonmail.com

authors calculate $\langle \rangle$ through Fourier space methods, real space methods, or, instead, they use Monte Carlo algorithms like Konstandin et al. (2012) and more recently Boneberg et al. (2015). However, the results from Monte Carlo calculations always stem from a partial use of the available data, which can produce severe errors. As we demonstrate here, Monte Carlo methods may not yield nor approximate correctly second order structure functions.² We directly prove this by simply comparing the second order structure function obtained from a real space method and Fourier space methods –which lead to correlation functions, see Schulz-Dubois & Rehberg (1981)– with the results of a Monte Carlo algorithm.

When normalised by $2 \sum_{i \in \mathcal{L}} u_i^2$, with \mathcal{L} being the finite spatial extension of the velocity field u , the normalised second order structure function $S_{2,n}(\delta r) \rightarrow 1$ for large enough δr ; in other words, the transversal S_2 has a well definite upper bound for large δr when the data have a finite extension.³ Taking this into account and by using robust Fourier and real space algorithms to analyse the Huygens region of M 42, we will be (up to our knowledge) the first to compute correctly the S_2 corresponding to its $H\alpha$ emission and make the corresponding analysis. The PPV cubes we analyse were obtained by Weilbacher et al. (2015).

The paper is organized as follows. In Section 2 we analyse the probability distribution function of the velocity field contained in the PPV cubes and select different thresholds for the minimum and maximum velocity to be considered. The previous allows to separate the image of the region in different segments of interest. In Section 3 we present the corresponding second-order structure functions. In Section 4 we discuss our results. The conclusions are presented in Section 5.

2 THE DATA

M 42 or the Orion Nebula, is one of the best and most studied Galactic H II regions and also the closest at a distance of approximately 440-pc. Because of that, it serves as a prototype for comparison with other H II regions. Its central region exhibits vigorous recent star formation and contains the densest nearby cluster of OB stars. The Nebula is located in front of the parent molecular cloud OMC-1, which makes it accessible for detailed study at all available wavelengths. Its ionized gas has been extensively studied spectroscopically in $H\alpha$ and the radio bands e.g. O’Dell & Harris (2010); van der Werf, Goss & O’Dell (2013). Because of the great quantity of studies done about it, the Orion Nebula has become central for our understanding of massive star formation and stellar feedback.

Recently, the ionised gas in the central Huygens region of M 42 (with an angular size of $\sim 5.9' \times 4.9' \approx 0.76 \times 0.63 \text{ pc}^2$) was surveyed by Weilbacher et al. (2015) in the wavelength range of 4595–9366 Å using integral field spectroscopy. They

² In the case of velocity fields with nice properties like isotropy, homogeneity or with symmetric simple PDFs it may be possible to obtain convergent structure functions but not in the general case because of the “mean field” effect discussed in Sections 2 and 4

³ in what follows we assume that S_2 is always normalised, so we will omit the subindex n

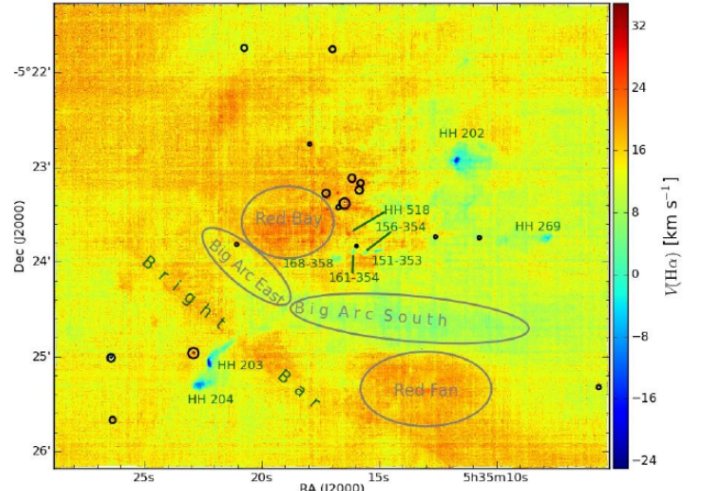


Figure 1. The Orion Nebula velocity field in $H\alpha$. The ellipsoids indicate the zones where the brightest stars reside. Image from Weilbacher et al. (2015).

obtained PPV maps in $H\alpha$ (see Figure 1) using the *MUSE* instrument at the ESO VLT. Their spatial resolution was $0.2''$. They also used the [N II] and [S III] lines to derive the mean electron temperature and found $T_e \approx 8500\text{--}9200 \text{ K}$. Outside the ionization front they found electron densities in the range $N_e \approx 500\text{--}10000 \text{ cm}^{-3}$. They also found that the layer of the ionization front has a higher electron density, $N_e \approx 25000 \text{ cm}^{-3}$.

Using *MUSE*, Weilbacher et al. (2015) were able to obtain 2D maps of the ionized gas velocity from Gaussian centroids of the $H\alpha$ and other emission lines. In $H\alpha$, they found that the strongest features in velocity space are close to Herbig-Haro objects present in the region, some stars and also in a few broad zones labelled as the Bright Bar, Red Fan, Red Bay, Big Arc East and Big Arc South, see Figure 1. The image size of the $H\alpha$ map in pixels is 1766×1476 . The length corresponding to one pixel is 0.00043-pc . In the map, the Herbig-Haro objects are marked with the label “HH”.

We obtained the un-normalised PDF (Probabilistic Distribution Function) of the raw $H\alpha$ data using 900 bins in order to make the secondary cusp to the left of the main central peak visible. The PDF is shown on Figure 2a. One can observe a very cuspy central distribution with velocities between $u \approx 1\text{--}23 \text{ km s}^{-1}$, a small cusp between $v \approx -1\text{--}1 \text{ km s}^{-1}$ and broad heavy tails that expand up to $u \approx -400\text{--}400 \text{ km s}^{-1}$. Broad heavy tails are usually found in studies of the PDF of interstellar turbulence, see Federrath et al. (2010) and references therein. The mean of the data is $\mu_u = 14.38 \text{ km s}^{-1}$ and its standard deviation is $\sigma_u = 4.51 \text{ km s}^{-1}$.

Figures 2b and 2c show that the tails of the PDF are very heavy in comparison with those of the Gaussian fitted to the positive part of the central bicuspid region. The tails at the sides of this central region are discontinuous because they correspond to very small areas (from 1 to less than 10 pixels) with high positive or negative velocities. These very small areas are close to prominent features like Herbig-Haro objects and young stars, e.g. the small encircled region to

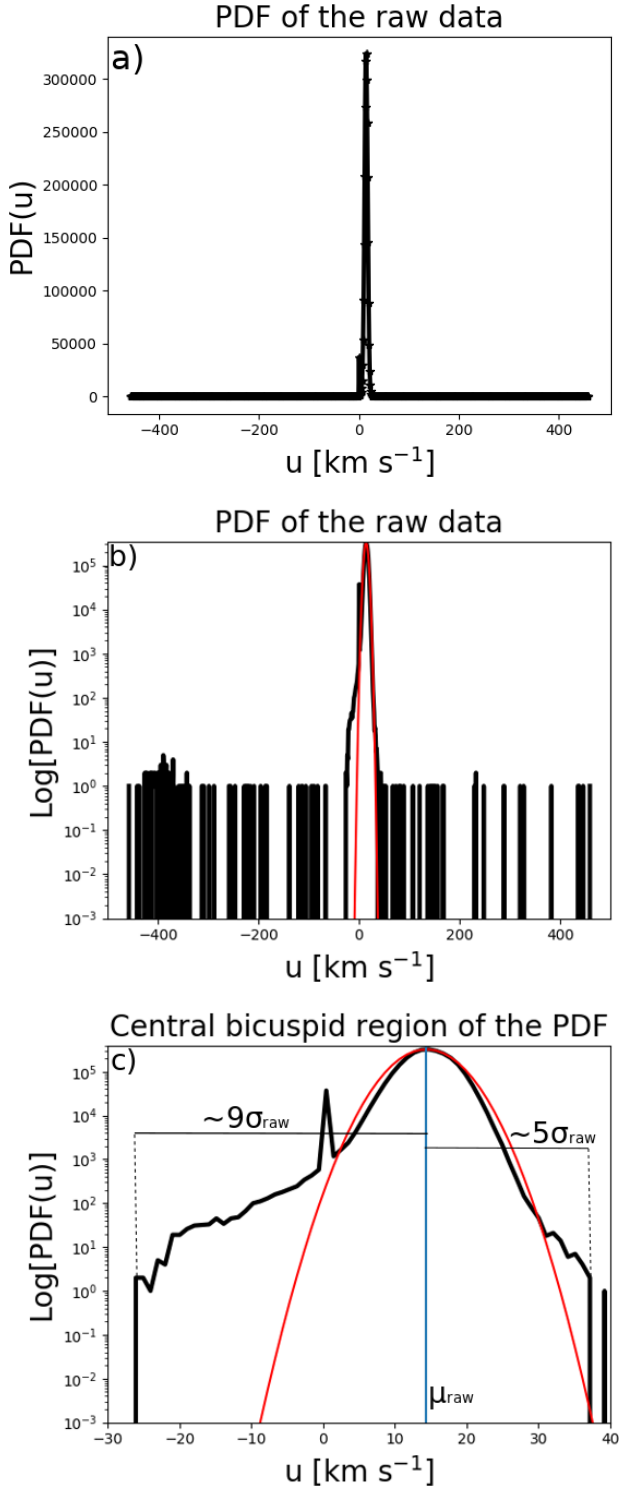


Figure 2. a) PDF of the raw velocity data in H α ; b) semi-logarithmic plot of the previous PDF. The red line represents a Gaussian used as a reference fitting for the central part of the main cusp. The Gaussian has the same mean and standard deviation than the data within $-5\sigma/5\sigma$ from the raw data mean. The amplitude of the Gaussian was set to that of the tallest cusp; c) Zoom-in of the central bicuspid part of the PDF.

the Northwest of HH 203. On the other hand, all negative velocities in the central bicuspid region correspond to small areas close to Herbig-Haro objects like HH 202, HH 203, HH 204 and HH 269. The areas of the regions with negative velocities associated to the negative side of the central bicuspid region are larger than those associated to the discontinuous broad tails surrounding it.

It is noticeable that the left tail of the central bicuspid region is broader than the right one. This asymmetry has also been observed in PDFs obtained from numerical simulations of solenoidal and compressive turbulence, see figure A1 in Federrath (2013). However, differences between Figure 2c and figure A1 in Federrath (2013) are that, comparatively, the left tail in Figure 2c is significantly broader than the right tail, it decreases much less rapidly and it has a secondary cusp. Nevertheless, except by these differences, the overall profile of the central bicuspid region of the PDF is consistent with that presented in figure A1 in Federrath (2013), in particular with the curve corresponding to solenoidal turbulence.

The broad central sides of the central bicuspid region are important in determining the exponent of the inertial range of the second order structure function, much more important than the discontinuous tails at the sides, see Section 3. Thus, because of the long tails of the PDF, the data need to be filtered out in order to better understand the distribution around the two central cusps (in linear scale) and its relation with the observed spatial distribution of velocities. We consider the next four cases.

Filter 1

We filtered out the data such that only velocities within $-9\sigma/5\sigma$ from the mean of the raw data are considered. This filters out the discontinuous tails. We used this time 120 bins for visualization purposes. The resulting PDF is shown in Figure 3a. The corresponding map, shown in Figure 4a basically coincides with the map published by Weillbacher et al. (2015). The zones marked out in their figure as the Big Arc East, the Big Arc South, the Bright Bar, the Red Bay and the Red Fan are all present as well as the general morphology of the field. However, now we have gained more insight about the PDF. This time, one can observe very clearly the central cusp between $u \approx 1 - 23$ km s^{-1} followed by a heavy positive tail from $u \approx 23 - 37$ km s^{-1} . A secondary cusp between $u \approx -1 - 1$ km s^{-1} followed by a heavy tail from $u \approx -1 - (-26)$ km s^{-1} can also be observed. The mean of the filtered PDF is $\mu_u = 14.39$ km s^{-1} and the standard deviation is $\sigma_u = 3.72$ km s^{-1} . The invariance of the mean implies that the raw-data long tails of up to ± 400 km s^{-1} do not contribute significantly to the bulk of the PDF but their absence decreases the standard deviation by $\sim 18\%$.

Filter 2

We noticed that negative and small positive velocities are present only on the light blue zones of the map, i.e. in the Big Arc South and close to the Herbig-Haro objects. This might indicate that the gas contained there is uncoupled from the large-scale motion in the rest of the Huygens region. The motion in the Big Arc South may be indeed only associated to the Herbig-Halo objects and several bright stars. This is important to know at the time of calculating structure functions because it would not make sense to calculate a single structure function for two regions with uncoupled dynamics, i.e. in the case of using only the raw data or the

data filtered out to $-9\sigma/5\sigma$. Because of this we filtered the PPV image to $-1\sigma/5\sigma$ which completely removes the singular negative tail of the distribution presented in Figure 3a. The resulting distribution is presented in Figure 3b, its mean is $\mu_u = 15.11 \text{ km s}^{-1}$ and its standard deviation is $\sigma_u = 2.80 \text{ km s}^{-1}$. The mean increases because we masked the small and negative values corresponding to the blue zones leaving only larger velocities, which produce also a smaller standard deviation. The corresponding image is shown in Figure 4b. One can see there that all the blue zones including the Big Arc South have been completely filtered out (white dots).

Filter 3

We decide also to analyse separately the blue zones in the map since we have shown above that they correspond to the negative tail of the $-9\sigma/5\sigma$ distribution and seem to manifest an uncoupled motion. Such broad negative-end tail is presented in Figure 3c and has a mean of $\mu_u = 6.65 \text{ km s}^{-1}$ and a standard deviation of $\sigma_u = 3.70 \text{ km s}^{-1}$. The corresponding image is shown in Figure 4c.

Filter 4

Finally, we filtered the data up to $-1\sigma/1\sigma$ which yields a mean of $\mu_u = 14.53 \text{ km s}^{-1}$ and a standard deviation of $\sigma_u = 2.27 \text{ km s}^{-1}$. The resulting PDF extends from 9-19 km s^{-1} . In this case, many pixels belonging to the Big Arc South, Big Fan, Big Bay and the Bright Bar are masked (see Figure 4d). In the next section, we will show through structure functions that the unmasked yellow and red regions are responsible of providing most of the energy for the turbulent motion, even when the turbulence is more violent in the zones that correspond to the broad positive tail of the $-9\sigma/5\sigma$ distribution. This positive broad tail corresponds to the Red Fan, the Red Bay, an important part of the Bright Bar and an important part of the large region in the Northwest. We regard these $-1\sigma/1\sigma$ masked field as a "mean field" that represents the background velocity field once the most prominent features have been eliminated.

3 STRUCTURE FUNCTIONS

A nebular analysis of the central part of the Orion Nebula (the Huygens region) was carried out by [McLeod et al. \(2016\)](#) using the same MUSE integral-field observations than here. They also attempted to diagnose the turbulence in the region using second order structure functions. For the latter, they used the Monte Carlo algorithm of [Boneberg et al. \(2015\)](#) using only a sample of 10^3 pixels whereas the data consists of $> 2 \times 10^6$ pixels.

Here, we are particularly interested in the structure of the projected velocity field obtained through the $\text{H}\alpha$ emission line since it allows to diagnose turbulent motions from 0.00043-pc (the length covered by one pixel) up to 1-pc. The area of the central region of the Nebula is roughly $0.76 \times 0.63 \text{ pc}^2$, but we perform an analysis up to $\delta r \approx 1\text{-pc}$ to probe the convergence of the S_2 's. For calculating the structure function we use the full data, i.e. we use every pixel of the map. We calculate the S_2 's using both a real space algorithm and the standard Fourier space algorithm.

On Figure 5a, we present the normalised second order structure functions of the raw data and the filtered datasets. We can see that the S_2 's corresponding to the raw data, the $-9\sigma/5\sigma$ filtered data and the $-1\sigma/5\sigma$ filtered data look

Table 1. Power laws to which the data was fitted. Their intervals of validity are given in pixels; one just needs to multiply by 0.00043 to convert to pc. The percent of the total energy corresponding to each dataset is also given.

Dataset	Fitted power-law	interval of validity	R^2	% energy
raw	$0.004656 \times \delta r^{0.7287}$	300-1500	0.9997	100.00%
$-9\sigma/5\sigma$	$0.003338 \times \delta r^{0.7668}$	300-1500	0.9995	97.30 %
$-1\sigma/5\sigma$	$0.006191 \times \delta r^{0.6824}$	300-1500	0.9998	95.16%
$-9\sigma/-1\sigma$	$0.01172 \times \delta r^{0.08526}$	1-1500	0.9818	2.14%
$-1\sigma/1\sigma$	$0.01271 \times \delta r^{0.5566}$	300-1500	0.9996	78.68%

similar for $\delta r > 300$ pixels. This occurs because the corresponding datasets have very similar (close to 100%) kinetic energies per unit mass, k . The percentage of k is obtained by multiplying the asymptotic value of each normalised S_2 by 100. In Table 1, we give the percent of kinetic energy per unit mass that corresponds to each curve. We used the raw data as a reference. One can see that the $-1\sigma/1\sigma$ filtered data (green line) contains $\sim 79\%$ of k . This shows that the regions where the most violent turbulent motion occurs (the Red Fan, the Red Bay, the Bright Bar and a significant part of the large region to the Northwest of the image) contribute only with $\sim 16\%$ of k . These regions correspond statistically to the broad positive tail of the PDF. Despite being large, the extended blue zone contributes only with $\sim 2\%$ of k . The discontinuous long tails contribute with $\sim 3\%$ of k .

With exception of the $-9\sigma/-1\sigma$ dataset, all the curves have initial segments that do not correspond to power laws (see Figure 5b). Furthermore, a power law can be fitted from $\delta r = 1$ to $\delta r = 1500$ pixels only to the $-9\sigma/-1\sigma$ dataset. Nevertheless, we found that from $\delta r = 300$ pixels (0.129-pc) to $\delta r = 1500$ pixels⁴ (0.645-pc) power laws of the form ax^b describe well the shape of the other S_2 's. The amplitude and exponents of these power-laws are given in Table 1.

4 DISCUSSION

As considered by [McLeod et al. \(2016\)](#), the turbulence in the Huygens region generates a velocity field characterised by stochastic hierarchical fluctuations that can be analysed through second-order structure functions. They calculated $S_2(\delta r)$ in real space using the Monte Carlo algorithm of [Boneberg et al. \(2015\)](#). Unfortunately, because of the random sampling characteristic of the algorithm, their calculation was incomplete and erroneous since they only used a sample of 10^3 pixels for calculating S_2 , while the MUSE dataset consists of more than 2.6×10^6 pixels. Because of the above, for the $\text{H}\alpha$ velocity map, they obtained an exponent of $b = 0.41\text{--}0.45$ for their computed S_2 .

In turn, we found an exponent $b \sim 0.73$ for the raw data and of $b \sim 0.77$ for the $-9\sigma/5\sigma$ filtered data. The fact that the former exponent is smaller than the latter is due to the fact that the former has associated a larger amplitude a such that the respective S_2 is always larger than the latter for any given δr . Both exponents indicate a turbulence more

⁴ which is approximately the size of the North-South side of the data-box

violent than the isotropic homogeneous turbulence defined by Kolmogorov, which has $b_K = 2/3$, Kolmogorov (1991). Nevertheless, by the evidence provided by the PDF analysis we performed and also by visual analysis, the blue zones in the map seem to be uncoupled from the dynamics of the rest of the map. Statistically, the blue zones correspond to the broad negative tail of the PDF and it includes a small secondary peak. If such a tail is removed, as in the case of the $-1\sigma/5\sigma$ filtered data the blue zones would not participate in the calculation of S_2 and one would obtain an exponent $b \sim 0.68$, which is only slightly larger than the exponent $2/3$ predicted by the Kolmogorov theory.

The previous contradicts the conclusion of McLeod et al. (2016) which blamed the spectral and spatial resolution of MUSE for the small exponents they obtained. They also pointed out that because of that, they were not able to reproduce the structure functions of previous works. However, two things must be remarked: a) first, they did not obtain the right exponents because of the Monte Carlo algorithm they used not because of the MUSE resolution and b) second, the exponents obtained in the previous works they cited are flawed since they come from S_2 's that were evidently miscalculated, e.g. they do not display an asymptotic limit for large δr . So, we do not know neither the correct exponents for the data of previous works because of miscalculations. We suggest that a re-calculation and a re-analysis of the data of previous works would be useful.

In our case, we find that when the negative broad tail of the PDF is ignored (the blue zone) and the positive tail is conserved, the yellow and red zones seem to exhibit an S_2 similar to that predicted by Kolmogorov for incompressible, homogeneous isotropic turbulence. This seems to indicate that the effect of compressibility is small in this case. Notice that the Red Fan, the Red Bay, the Bright Bar and the large zone at the Northwest of the image are prominently visible only when the positive broad tail is taken into account, compare Figures 4a and 4b with Figure 4d. The latter Figure, which corresponds to the $-1\sigma/1\sigma$ filtering, can be thought as the representation of a "mean field" without the clustering structure produced by high velocity regions (red zones). These high velocity clusters correspond statistically to the positive tail of the PDF and they are responsible of making the exponent of the $-1\sigma/5\sigma$ filtered data (Figure 4b) almost coincide with the exponent of Kolmogorov turbulence. If the positive tail is also ignored we obtain the "mean field" which has an exponent $b = 0.5566$ which is below the exponent of Kolmogorov turbulence.

By using a Monte Carlo algorithm, McLeod et al. (2016) did skip the contribution of the positive broad tail and thus obtained something similar to our data with a $-1\sigma/1\sigma$ filtering, which has an exponent b below $2/3$. The difference is that their 'unintentional' filtering due to the Monte Carlo algorithm they used was more drastic than our $-1\sigma/1\sigma$ "mean field" filtering. That is the reason why sometimes the results from Monte Carlo algorithms are not reliable: they can induce a very drastic "mean field" filtering.

Finally, we remark that the blue zones enhance the contrast between velocities and because of that we obtain sharper S_2 's, however this is an effect that we do not need to consider if the dynamics of the blue zones is really detached from the dynamics of the rest of the gas. The blue zone per se has an S_2 which can be described by a power

law of the form ax^b from $\delta r = 1$ pixel to $\delta r = 1500$ pixels. However the exponent corresponding to such region is very small, $b = 0.0861$ and the region contains only 2.18% of the kinetic energy per unit mass.

5 CONCLUSIONS

We have calculated the second order structure functions of the Huygens Region of M 42 taking into account the velocity PDF of the PPV cubes we analysed. We found that when all the data in the map is considered, one can forecast a turbulence more violent than Kolmogorov turbulence since the slope of the inertial range is $0.72-0.77$. On the other hand, we found that if we ignore the zones that correspond to the broad negative tail of the velocity PDF we obtain an exponent of 0.6824 , which is close to $2/3$, the exponent for Kolmogorov turbulence. So, according to our diagnostic the gas exhibits a motion between Kolmogorov-type turbulence ($b = b_K = 2/3$) and Burgers turbulence ($b = 1$), see Bouchaud, Mézard & Parisi (1995) and Federrath (2013). Furthermore, the structure function of the raw data and the $-9\sigma/5\sigma$ filtered data are very close to the observational Larson law which generalises to $S_2 \sim \delta r^{0.74-0.76}$. The previous law have been found in Kolmogorov-Burgers turbulence where the dissipative structures are quasi-one dimensional shocks, see Boldyrev (2002) and references therein. Nevertheless, in our case we do not have a Kolmogorov-Burgers regime but two separated regimes: an almost Kolmogorov regime and a secondary regime with a small exponent for the inertial regime and where bright stars and Herbig-Haro objects are present (the blue zone on Figure 1).

The analysis of the velocity map by segmentation using the velocity PDF is one of the differences of our work with previous ones. Another difference is that we obtained the second structure functions both in Fourier and real space paying attention to every detail important for their calculation. Because of that our results are robust and reliable.

Finally, we suggest that the velocities in the negative tail of the PDF correspond to an extended region of ongoing star formation that has undergone local gravitational collapse, see Klessen, Heitsch & Mac Low (2000). The presence of Herbig-Haro objects only in this extended region as well as the presence of bright stars in the Big Arc South support this hypothesis.

6 ACKNOWLEDGEMENTS

We thank Dr. Peter Weilbacher for kindly providing the PPV cubes that made this study possible. We also thank him for giving permission to reproduce an image (Figure 1) from Weilbacher et al. (2015). We also thank our anonymous referee whose recommendations helped to greatly improve this paper.

REFERENCES

- Anorve-Zeferino G. A., Tenorio-Tagle G. & Silich S., MNRAS, 2009, 394, 1284
- Anorve-Zeferino G. A., MNRAS, 2016, 463, 84
- Boldyrev S., ApJ, 569, 841

- Boneberg D. M. et al., MNRAS, 447, 1341
 Bouchaud J. P., Mézard M. & Parisi G., PhysRevE, 52, 3656
 Federrath C., Klessen R.S. & Schmidt W., ApJ, 2009, 692, 364
 Federrath C. et al., A&A, 2010, 512, 81
 Federrath C. & Klessen R. S., ApJ, 2012, 761, 156
 Federrath C., MNRAS, 2013, 436, 1245
 Federrath C. et al., IAUS, 2017, 322, 123
 Glover S. C. O. et al., 2010, MNRAS, 404, 2
 Gritschneider M. et al., 2009, ApJ, 694, 26
 Harquist T. W., Pittard J. M. & Falle S. A. E. G., Diffuse Matter from Star Forming Regions to Active Galaxies, A Volume Honouring John Dyson, Springer, 2007, 103
 Klessen R. S., Heitsch F., Mac Low M.-M., 2000, ApJ, 535, 887
 Klessen R. S., 2001, ApJ, 556, 837
 Kolmogorov A. N. et al., 1991, Royal Soc. Proc. A, 434, 9
 Konstandin L. et al., 2012, J. Fluid Mech., 692, 183
 McLeod A. F. et al., 2016, MNRAS, 455, 4057
 Mellema G. et al., 2006, ApJ, 647, 397
 O'Dell C. R. & Harris J. A., 2010, AJ, 140, 985
 Schulz-Dubois E. O. & Rehberg I., 1981, Appl. Phys., 24, 323
 Tremblin P. et al., 2012, A&A, 546, 33
 van der Werf P. P., Goss W. M. & O'Dell C. R., 2013, ApJ, 762, 101
 Weilbacher P. M. et al., 2015, A&A, 582, 114

This paper has been typeset from a $\text{\TeX}/\text{\LaTeX}$ file prepared by the author.

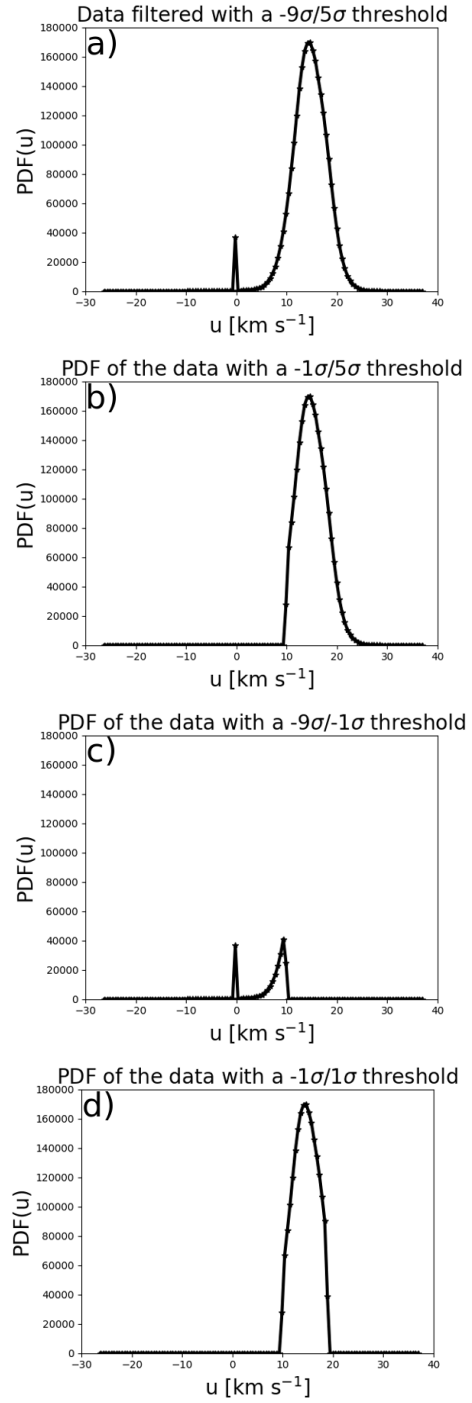


Figure 3. PDF of the velocity field in $\text{H}\alpha$: a) PDF of the data filtered out using a $-9\sigma - 5\sigma$ window centred in the mean of the raw data; b) PDF without the negative broad tail corresponding to a $-1\sigma/5\sigma$ filtering; c) PDF of the blue region corresponding to a filter of $-9\sigma/-1\sigma$; and d) PDF of the data filtered out to $-1\sigma/1\sigma$ of the mean of the raw data

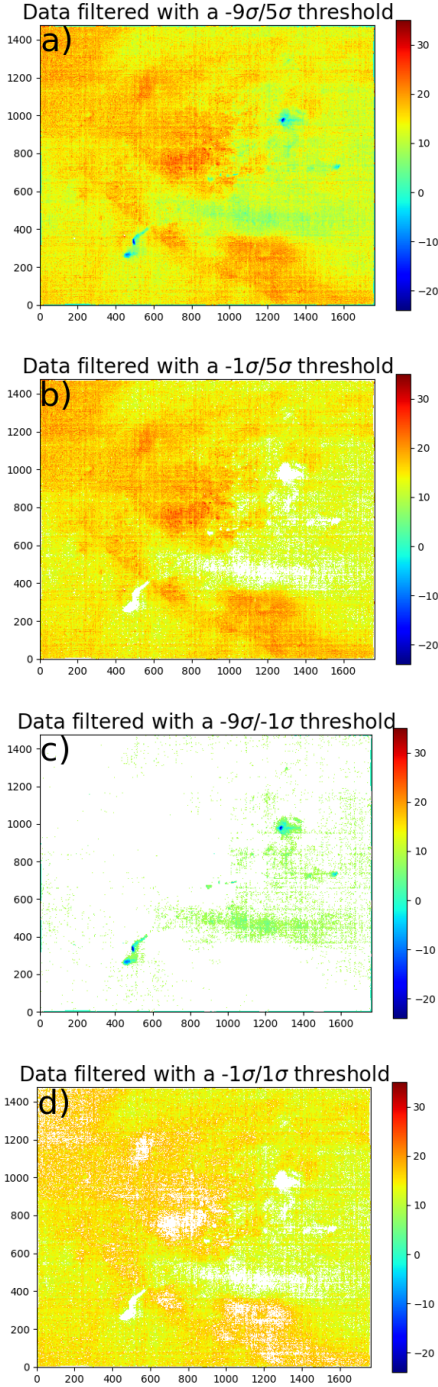


Figure 4. filtered H α maps: a) map filtered using a $-9\sigma - 5\sigma$ threshold; b) map filtered using a $-1\sigma/5\sigma$ threshold; c) map corresponding to the blue zone ($-9\sigma/-1\sigma$ filtering); and d) map corresponding to a $-1\sigma/1\sigma$ filtering.

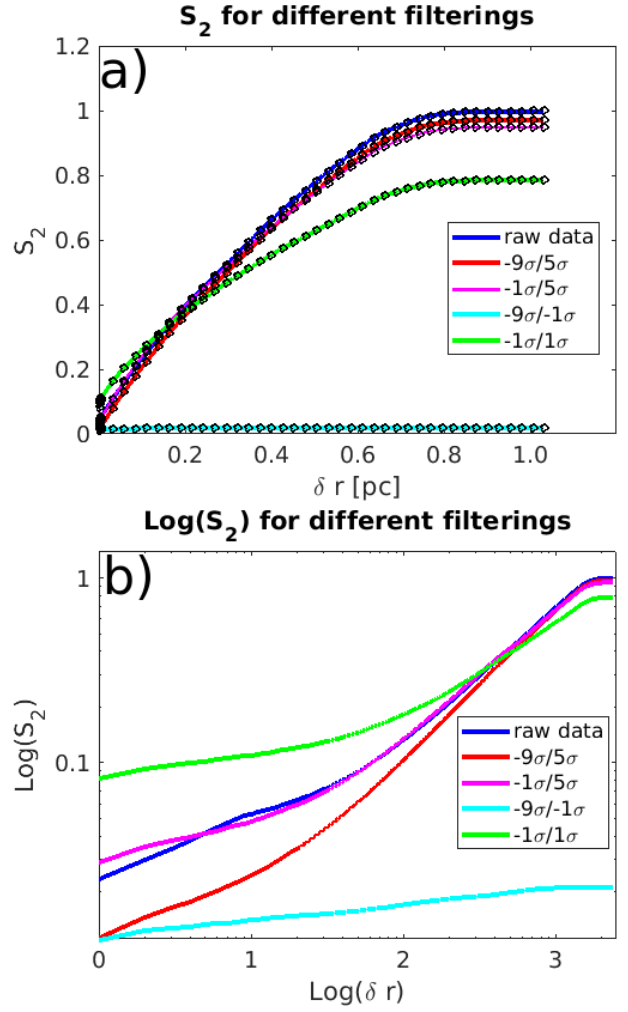


Figure 5. Normalised S_2 's of the raw and filtered velocity data in H α . The solid lines correspond to S_2 's computed by Fourier space methods. The black circles correspond to S_2 's calculated using a real space algorithm. a) S_2 in linear scale with the x-axis in pc b) S_2 in logarithmic scale with the x-axis in pixels